ACS APPLIED MATERIALS & INTERFACES

Research Article

www.acsami.org

Atomic Layer Deposited Molybdenum Nitride Thin Film: A Promising Anode Material for Li Ion Batteries

Dip K. Nandi,[†] Uttam K. Sen,[†] Devika Choudhury, Sagar Mitra,* and Shaibal K. Sarkar*

Department of Energy Science and Engineering, IIT Bombay, Mumbai, Maharashtra 400076, India

Supporting Information

ABSTRACT: Molybdenum nitride (MoN_x) thin films are deposited by atomic layer deposition (ALD) using molybdenum hexacarbonyl [$Mo(CO)_6$] and ammonia [NH_3] at varied temperatures. A relatively narrow ALD temperature window is observed. *In situ* quartz crystal microbalance (QCM) measurements reveal the self-limiting growth nature of the deposition that is further verified with *ex situ* spectroscopic ellipsometry and X-ray reflectivity (XRR) measurements. A saturated growth rate of 2 Å/cycle at 170 °C is obtained. The deposition chemistry is studied by the *in situ* Fourier transform infrared spectroscopy (FTIR) that investigates the surface bound reactions during each half cycle. As deposited films are amorphous as observed from X-ray diffraction (XRD) and transmission electron microscopy electron diffraction (TEM ED) studies, which get converted to hexagonal-MoN upon annealing at 400 °C under NH_3 atmosphere. As grown thin films are found to have notable potential as a carbon and binder free anode material in a Li ion battery. Under half-cell configuration, a stable discharge capacity of 700 mAh g^{-1} was achieved after 100 charge−discharge cycles, at a current density of 100 μA cm^{-2}.

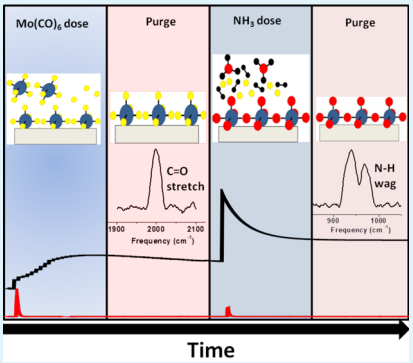

KEYWORDS: *atomic layer deposition, Li ion battery, FTIR, molybdenum nitride, quartz crystal microbalance*

INTRODUCTION

For its diverse chemical composition and different crystalline phases,[1−3] molybdenum nitride has been found applicable in a wide range of applications such as Cu diffusion barrier layer in microelectronics and optoelectronics[4,5] and also in fuel cells as catalyst.[6] Its recent use in tribological applications has opened up particular interests both in research and in industries.[7,8]

Thin films of molybdenum nitride have been deposited through various processes. Probably, simplest among all is to convert its oxides to nitrides in a controlled N_2+H_2 or NH_3 atmosphere at elevated temperature.[9−11] Other processes that have been mostly studied include physical vapor deposition by reactive or DC magnetron sputtering.[7] Though chemical vapor deposition (CVD and MOCVD) of molybdenum nitride films has come into play lately, it has gained popularity as an important technique to deposit transition metal nitrides.[12,13]

Atomic layer deposition (ALD), earlier known as atomic layer epitaxy (ALE), is considered as a modified CVD where the reactants are introduced sequentially to the reactor and the growth is found to be self-limiting. These self-limiting traits of the reactions offer excellent control over the film deposition at a monolayer level and craft conformal coatings on high aspect ratio structures. The advantages of ALD lie in the deposition of a vast horde of thin film binary compounds.[14] Recently, attributes of ALD have been vastly exploited to produce a potpourri of materials such as oxides extending to rare earth elements,[15−17] sulfides,[18−20] pure metals,[21,22] and even organic−inorganic polymers.[23−25]

ALE of molybdenum nitride was first reported by using its halide ($MoCl_5$) compound.[26] Later metal organic precursors such as bis(tert-butylimido)-bis(diethyl(isopropyl)amido)-molybdenum [$(tBuN)_2Mo(NEt_2)_2$] and its derivatives were used for ALD.[27] Use of metal organic precursors not only avoids corrosive reaction products such as HCl or HF but also reduces the deposition temperature. Furthermore, it enhances the volatility of the metal precursors that ease the vapor transport to the reaction vessels. Recently, ALD of MoO_3 and Co−Mo mixed oxides from molybdenum hexacarbonyl [$Mo(CO)_6$] opened a newer direction in deposition of Mo compounds.[28,29] In this paper, we have further explored its diversity to deposit molybdenum nitride films aiming for its application in electrochemical storage.

The use of metal nitrides in lithium ion battery was started in the early 1990s when layered lithiated transition metal nitrides were used as host matrix for lithium ion intercalation,[30−32] but the use of layered lithtiated metal nitrides did not get more attention due to its poor electrochemical activity. However, with the discovery of the conversion based mechanism[33] in the year 2000, the metal nitrides again came into the picture and the electrochemical performances of Zn_3N_2, Cu_3N, and Ge_3N_4 with lithum were demonstrated.[34,35] Due to poor electrochemical stability of these metal nitrides, the study did not flourish much, but in recent years, transition metal nitrides have been gaining more interest as lithium ion battery anode due to two major advantages of nitride materials over metal oxides, (i) low polarization loss (due to decrease in the M−X bond

Received: January 14, 2014
Accepted: March 18, 2014
Published: March 18, 2014

   dx.doi.org/10.1021/am500285d | ACS Appl. Mater. Interfaces 2014, 6, 6606−6615

polarity) and (ii) better electronic conductivity of the end product (LiX_n) compared to oxides. It has been found in the literature that, by decreasing the M−X bond strength, polarization loss can be decreased from oxides to sulphides to phosphides and nitrides.[36,37] The major advantage of nitrides is that the end product of conversion reaction is Li_3N which is highly conductive.[38] As a result, several combinations of metal nitrides were tested as anode material in lithium ion batteries,[34,35,39−49] but the poor cyclic performance of most of these materials made them unappealing for further use. Materials like CoN, TiN, VN, and CrN however are found to exhibit better electrochemistry in comparison to others, and as result, more reports are available on these materials.[40,41,43−45]

Recent literature demonstrated that nitrided molybdenum oxide (MoO_2 annealed in NH_3) and molybdenum oxynitride show better electrochemical activity against Li in comparison to the pure molybdenum oxide.[50−53] Liu et al. explained the improved specific capacity with enhanced stability of nitrided-MoO_2 due to the better charge transport properties of the nitride materials at lower potential.[50] Similarly, Yoon et al. showed nitrogen doping in molybdenum oxide that results in better electrical conductivity and enhanced electrochemical performance than its oxide analogue.[51] It is to be noted that the electrochemical activity against Li ion in the above literature is strictly limited to the molybdenum oxide while nitrides only enhance the electronic conductivity.

Here, we report atomic layer deposition of molybdenum nitride films using molybdenum hexacarbonyl [$Mo(CO)_6$] and ammonia [NH_3]. *In situ* quartz crystal microbalance (QCM) was employed to study the film growth, complimented by other *ex situ* characterizations. The as deposited films that crystallized to hexagonal MoN upon annealing at an elevated temperature in NH_3 atmosphere were found to be amorphous. Electrochemical performance of the as grown films was tested as anode materials in Li ion battery. These thin film electrodes differed from the conventionally fabricated ones where usually binder and carbon are used to prepare the electrode. Under half-cell configuration, the as deposited ALD grown molybdenum nitride films showed good capacity retention capability against Li/Li^+. The reaction chemistry between molybdenum nitride (MoN_x) and lithium during the electrochemical cycling was analyzed with the help of electrochemical impedance spectroscopy.

EXPERIMENTAL SECTION

Material Synthesis. Deposition of MoN_x was carried out in a custom-built hot-wall viscous flow ALD reactor. A pressure of 1 Torr was maintained by a flow of 350 SCCM, 99.999% pure N_2 throughout the reaction time. Molybdenum hexacarbonyl (Gelest, USA) was used as the metal precursor for this deposition. NH_3 gas was used as nitrogen source that was directly fed to the reactor. The flow of NH_3 was controlled by a combination of metering valves and computer controlled pneumatic valves. Metal hexacarbonyl precursor was kept at room temperature and was dosed into the reactor using N_2 carrier gas with an overhead assembly. During deposition, the purging time between the two reactants was kept invariably at 15 s while the reactant dose times were varied. The reactor was equipped with Baratron capacitance manometer for pressure measurement and a rotary pump.

Material Characterizations. *In situ* quartz crystal microbalance (QCM) was employed to monitor the film growth. 6 MHz AT cut quartz crystals glued into a commercially available drawer and retainer assembly (Inficon) were placed horizontally to monitor the mass change. A mass resolution to ca. 1 ng was obtained under steady state condition.

In situ Fourier transform infrared spectroscopy (FTIR) measurements were performed in a different ALD chamber, similarly equipped as that previously. Infrared beam was fed to the chamber through ZnSe windows and recorded under absorbance mode. We used a liquid nitrogen cooled MCT detector with a Bruker Vertex-70 FTIR spectrometer for the measurements. All the reactions were performed on KBr palettes.

X-ray diffraction (XRD) and X-ray reflectivity (XRR) characterizations were performed with Bruker D8-Advance diffractometer equipped with Cu Kα cathode that emits at 1.54 Å. For diffraction measurements, films were deposited on microscopic glass substrate while for reflectivity experiments films were grown on single sided polished (111) Si wafers to minimize the interfacial roughness. Experimentally obtained XRR data were fitted with Parratt32 software to obtain the film thickness, roughness, and electron density. Furthermore, all thickness measurements were verified with spectroscopic ellipsometry (Sentech) measurements over a wavelength range of 350−850 nm at an incident angle of 70°, performed on the same or similar samples.

Elemental and compositional analyses were performed on a Thermo VG Scientific X-ray photoelectron spectrometer (MultiLab) equipped with Al Kα source (1486.6 eV). Peak fittings and analyses were executed using XPS peak 4.1 software. Before any analysis, peak positions were adjusted with respect to reference C-1s peak at 284.6 eV. High-resolution field emission transmission electron microscopy (HR-TEM, JEOL-2100F) along with a selected area electron diffraction (SAED) pattern was investigated to obtain microstructural information. Surface morphology was studied using a Veeco NanoScope IV MultiMode atomic force microscope (AFM) under semi-contact mode of operation.

Electrochemical Cell Fabrication. For all electrochemical measurements, films of ca. 200 nm thickness were grown on stainless steel substrate. Galvanostatic charge−discharge measurements were carried out in a coin-cell assembly having a cell configuration of Li/electrolyte/MoN_x. Cells were assembled inside an argon-filled glove box (Lab Star, Mbraun, Germany) with moisture and oxygen concentration levels of ca. 1 ppm. Lithium foil was used for both, counter and reference electrodes. Electrolyte consisting of 1 M $LiPF_6$ in EC/DMC (1:1 wt/wt) (LP-30, Merck, Germany) was used for all electrochemical measurements presented here. Borosilicate glass microfiber filters (Whatman) were used as a separator. A cycling voltammetry (CV) profile was obtained by measuring $i-V$ response at scan rate of 0.2 mVs^{-1} and swept within the voltage range of 0.01−3.0 V vs. Li/Li^+, using Bio-logic VMP-3. Electrochemical impedance spectroscopy (EIS) experiments were carried out at open circuit voltage (OCV) as well as at different potentials during the charge−discharge process, within a frequency range from 1 MHz to 0.01 Hz using Bio-logic VMP-3. Details of the process and the potentials were discussed in the Results and Discussions section. Electrochemical charge−discharge measurements were performed using Arbin Instrument, USA (BT2000 model) at a constant current density of 100 $\mu A\ cm^{-2}$. All electrochemical measurements were carried out at a constant temperature of 20°C to avoid any external perturbation.

RESULTS AND DISCUSSIONS

During the deposition, dosing and purging time sequences were represented by t_1, t_2, t_3, and t_4. Here, t_1 and t_3 were the dose time of molybdenum hexacarbonyl precursor and NH_3, respectively, while t_2 and t_4 were the purging times between the consecutive reactant doses, all in seconds. The deposition sequence was thus represented as t_1-t_2-t_3-t_4. Throughout this study, molybdenum nitride depositions were performed with the reaction sequence t_1-15-1-15, that implies t_1 seconds dose of the molybdenum hexacarbonyl while 1 s dose of NH_3 was maintained with 15 s purging in between. We found that the 1 s dose of NH_3 was relatively higher than a saturation dose; hence, variation of NH_3 pulse time or width is not reported here.

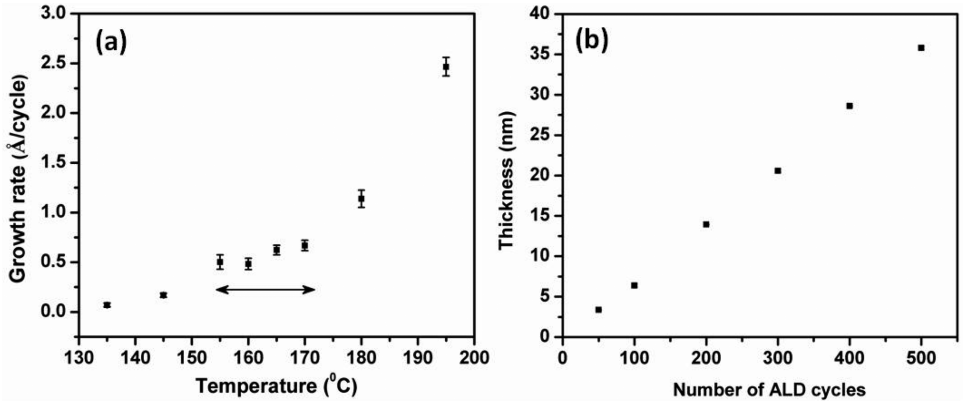

Figure 1. (a) Mass gain per single ALD (pulsing condition 1s-15s-1s-15s) cycle measured by *in situ* QCM study with increasing substrate temperature. (b) Thickness of the film with a pulsing condition of 1-15-1-15 measured by ellipsometry with the increasing number of ALD cycles MoN_x.

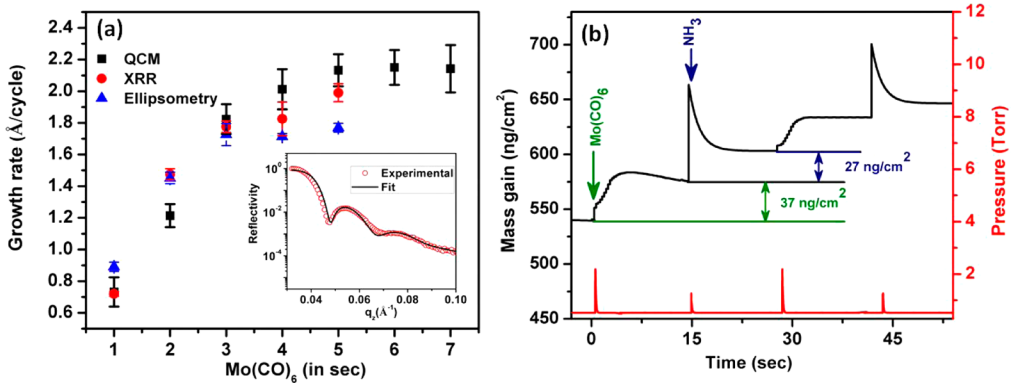

Figure 2. (a) Growth rate as calculated from QCM, XRR, and ellipsometry of the deposited films for a single NH_3 pulse with increasing dose time of $Mo(CO)_6$. (b) Mass gain for a complete ALD cycle from QCM measurements in the linear regime of the growth along with the corresponding pressure of the precursors.

Growth Characterizations. Figure 1a shows the growth rate, measured by *in situ* QCM, within the deposition temperature limit of 130−200 °C. The QCM essentially measures the change in the resonance frequency of the crystal due to the change in the deposited mass on it. The resultant mass gain was calculated from the frequency change of the piezoelectric crystal using the Sauerbrey equation. Between the temperature range of 155 and 170 °C, minimal variation in growth rate was observed which was within the experimental error regime. The growth rate obtained from the QCM mass gain under 1-15-1-15 pulsing condition was ca. 0.75 Å per cycle corresponding to an average mass gain of 36.5 ng cm^{-2}. The growth rate was calculated using the density of the film as 4.9 gm cm^{-3} found from the XRR measurements. An increase in the growth rate was observed at and beyond 180 °C corresponding to the dissociation of $Mo(CO)_6$.

The decomposition induced reaction beyond 180 °C was also confirmed by a large lateral gradient in the measured thickness of the as deposited films at different positions of the reactor. Lower growth rate in the temperature range below 150 °C was typically thermodynamically limited. We did not find any film growth below 130 °C. Thus, from the temperature window, 170 °C was chosen as the growth temperature for molybdenum nitride henceforth.

Figure 1b shows the MoN_x film thickness, measured by ellipsometry, as a function of the number of ALD cycles at 170 °C with the pulse sequence 1-15-1-15. The film thickness was found to have linear correlation with the number of ALD cycles and corresponded to an overall growth rate of ca. 0.75 Å per cycle.

To validate the ALD mechanism, *in situ* QCM was employed quantifying the self-limiting nature of the deposition. Figure 2a shows the measured growth rate with variation of the $Mo(CO)_6$ precursor dose. The growth per cycle was observed to level off at 2 Å per cycle after 4 s of metal precursor doses that yielded a total dose of 6.4×10^6 L. The self-limiting behavior as shown typically satisfied the basic requirements of atomic layer deposition. We have not shown the similar characteristics with varied NH_3 pulses that saturated from the first pulse itself, as also mentioned earlier. The saturation dose for NH_3 was ca. 7.5×10^5 L. The above observation univocally satisfied the self-limiting nature of each half cycle, and no further reaction took place with a greater number of reactant pulses.

The above obtained self-limiting nature of the ALD reaction was further verified with *ex situ* XRR and spectroscopic ellipsometry measurements. For XRR measurements, films were deposited on polished Si wafer with 300 cycles of reaction. Experimentally obtained Kiessig fringes along with the fitting model that includes 20 Å SiO_2 and the metal nitride layer are as shown in the inset of Figure 2a. The program fits individual densities and thickness of each layer separately. Density of the MoN_x films from the XRR fits was found to be ca. 4.9 gm cm^{-3}, which is substantially lower than the bulk value of either Mo_2N

dx.doi.org/10.1021/am500285d | ACS Appl. Mater. Interfaces 2014, 6, 6606−6615

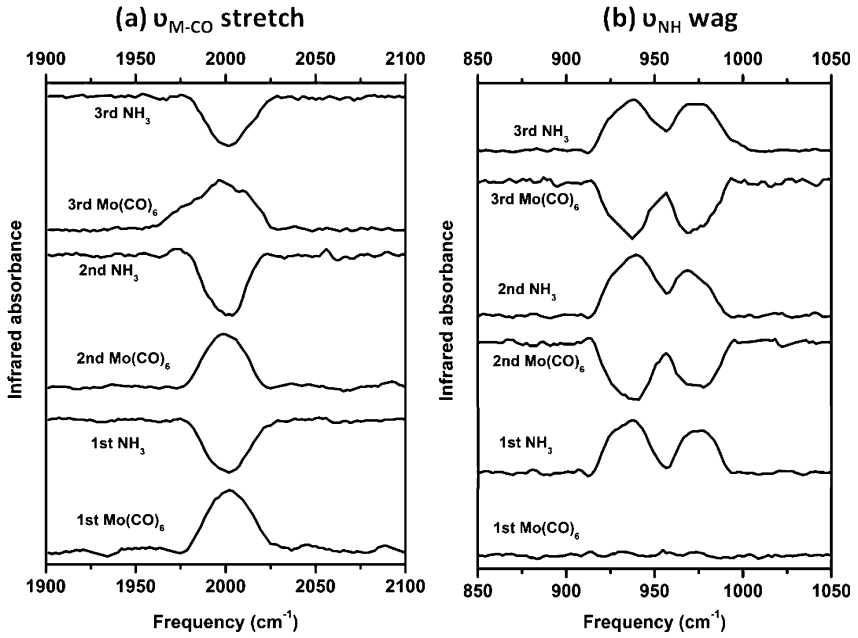

Figure 3. FTIR difference spectra of (a) M−CO stretch and (b) $-NH_2$ twist recorded during alternate dosing of the precursors.

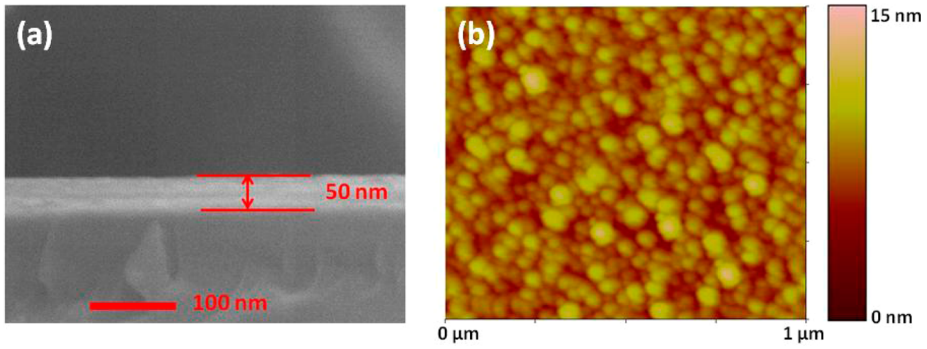

Figure 4. (a) Cross-section SEM image on Si wafer (b) surface AFM image after 300 ALD cycles.

or MoN. This discrepancy could be attributed to the amorphous nature of the deposit.

Mass change measured with QCM was further explored to investigate the half cycle reactions during the ALD process. Figure 2b shows a couple of cycles from the linear growth regime of MoN_x deposition with a 2 s dose of $Mo(CO)_6$ and a single dose of NH_3 with 15 s purging in between. The $Mo(CO)_6$ exposure resulted in a pronounced mass gain of ca. 37 ng cm^{-2} per cycle and was found to be reproducible within limited experimental error. The total mass change after the NH_3 exposure was found to be 64 ng cm^{-2} per cycle. Considering the density obtained from the XRR measurements as 4.9 g cm^{-3}, calculated growth rate was 1.2 Å per cycle that was consistent with the average mass gain obtained, as shown in Figure 2a for 2-15-1-15 pulsing sequence.

***In Situ* FTIR.** An *in situ* Fourier transform infrared (FTIR) spectroscopy study was performed to monitor the vibration spectra of the surface bound species after each ALD half cycle during the molybdenum nitride deposition. All spectra were measured at 170 °C under saturated dose condition. Figure 3 shows the difference FTIR absorption spectra that were obtained by subtracting the previous spectrum. Hence, the positive spectra indicate the addition of surface species while the negative spectra indicate the removal of the same. The spectra shown here were taken on a 50 cycles molybdenum nitride coated KBr palette. At around 2000 cm^{-1}, absorption corresponding to the M−CO stretch was observed after the $Mo(CO)_6$ dose.[54] The clear presence of the carbonyl group after the $Mo(CO)_6$ dose indicated the presence of the adsorbed surface species during the 1st half reaction. A symmetrical negative spectrum after the saturated NH_3 dose indicated a complete removal of the carbonyl group.

The complete removal under saturated dose condition was indicative of the relatively higher growth rate and carbon (impurity) free material. Complementary information could be found from the existence of the NH_2 surface species. The vibration spectra at around 950 cm^{-1} corresponds to the NH_2 twist that appeared after saturating dose of NH_3 and was found to be stepwise perfectly reciprocal to that of the carbonyl peak as shown in Figure 3b.[55] Even here, the positive difference spectra indicated the appearance of the NH_2 species while the negative spectra that appeared after the $Mo(CO)_6$ dose indicated the removal of the same species.

In view of the above observations, we hypothecate the deposition chemistry as stated below. For atomic layer deposition, the overall reaction was split into two separate half-reactions:

dx.doi.org/10.1021/am500285d | ACS Appl. Mater. Interfaces 2014, 6, 6606−6615

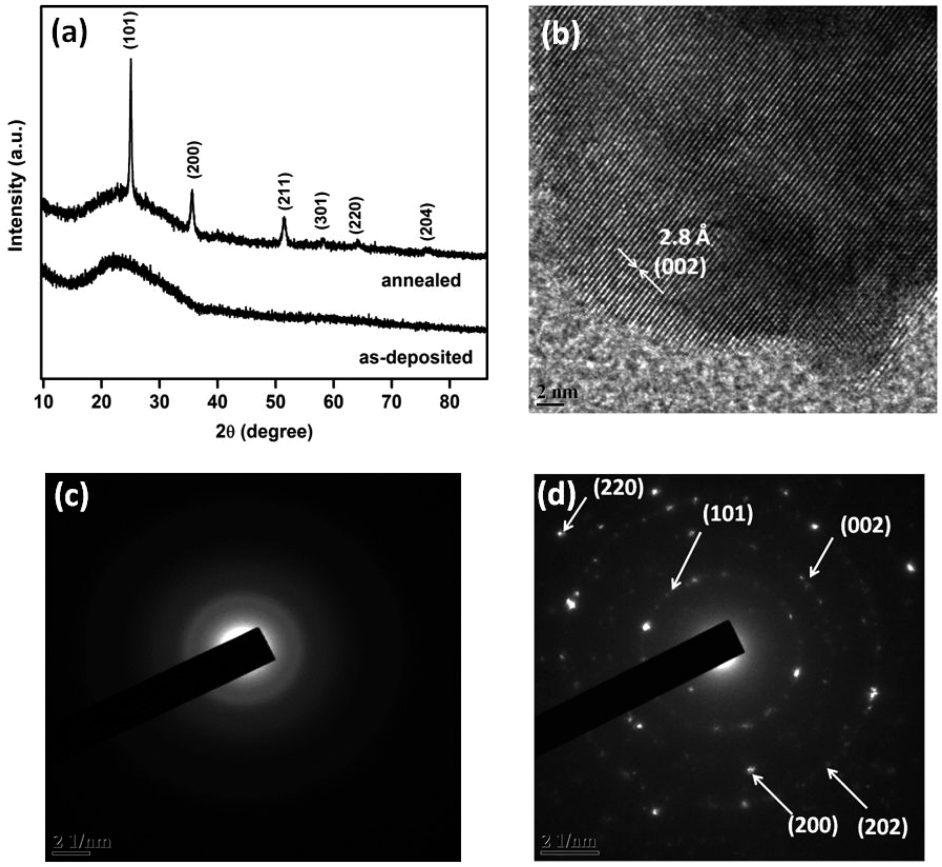

Figure 5. (a) XRD of as deposited film and after annealing at 400 °C under NH_3 atmosphere, (b) HRTEM image of the annealed film showing the lattice array of hexagonal MoN, (c) SAED for the as deposited film, and (d) SAED of the annealed film showing the co-centric fringes correspond to the planes of hexagonal MoN.

$$Mo(CO)_x^* + NH_3 \rightarrow Mo{-}NH_y^* + nH_2 + mCO \quad (1)$$

$$Mo{-}NH_y^* + Mo(CO)_6 \rightarrow MoN{-}Mo(CO)_x^* + nH_2 + mCO \quad (2)$$

where "∗" denotes the surface species.

The above mechanism, however, never outmoded other reaction pathways that could possibly explain the overall reaction. As shown above, in each half reaction (equations 1 and 2), the gaseous precursor species reacts with the surface bound species. Figure 3a showed the flip-flop appearances of the carbonyl peak that indeed indicates the second surface half-reaction, equation 2. Highly complementary information was obtained from the appearance−disappearance nature of the $-NH_2$ signature peaks as shown in Figure 3b that depicted the first half-reaction, equation 1. Thus, a combination of the above two half-cycles completed the ALD reaction during the molybdenum nitride film growth. Since the reaction continues until every surface species converts to a newer surface species, we limited our experiments under saturated dosage. The gaseous reactants along with the products were pumped out of the reactor. It ensured complete surface limited reaction that was indeed a rate-limiting factor of the ALD process. Incorporating simultaneous reaction sequences produces the molybdenum nitride film growth.

Film Characterizations. Low surface roughness was evident in the as deposited films on Si from morphological investigations, carried out with AFM. Figure 4b shows the surface morphology of the film of 24 nm thicknesses corresponding to 200 cycles of film growth, deposited at 170 °C. The RMS roughness of ca. 1 nm was estimated from an AFM scan on 1 × 1 μm^2 area. The cross-section SEM image also validated a uniform deposition after 400 cycles. The obtained thickness of 50 nm was found to be in close proximity to that obtained from QCM measurements (48 nm).

Films grown within the thermal ALD window regime were found amorphous from the X-ray diffraction (XRD) measurement and selected area electron diffraction (SAED) analysis. For TEM measurements, films deposited on microscopic glass substrates were scratched out and transferred to the grid. The broad wide ring in the SAED pattern and a featureless XRD pattern clearly indicated the absence of any long range ordering in the as deposited films as shown in Figure 5c,a. The hump around 25° corresponds to the effect of the microscope glass substrate. Annealing the same films at 400 °C under NH_3 atmosphere for 1 h converted them to hexagonal MoN. Diffraction peaks corresponding to the planes (101), (200), (103), (004), and (204) (JCPDS Card No. 00-025-1367) validated the crystallographic nature of the annealed film.

High-resolution TEM imaging also revealed the lattice fringes of the crystal, as shown in Figure 5b. The image showed the lattice array for (002) plane of hexagonal MoN having a d-spacing of 2.8 Å. The crystallinity of the annealed films was further confirmed by SAED that showed concentric fringes (Figure 5d) corresponding to the different planes of *h*-MoN with similar d-spacing matched with the same JCPDS card, mentioned earlier. However, it is worth mentioning here

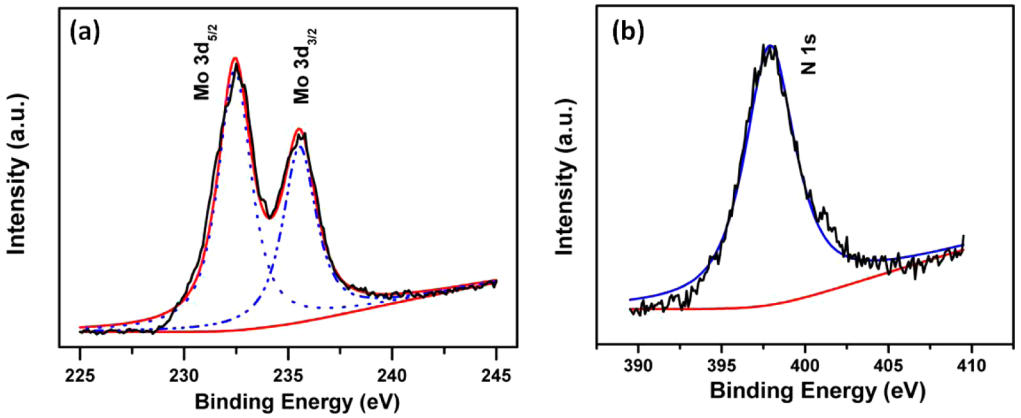

Figure 6. XPS of the as deposited film giving the characteristic peaks for (a) Mo3d and (b) N1s.

that lowering the annealing temperature or changing the ambient condition from NH_3 to N_2 or Ar never helped in crystallization.

We analyzed the chemical composition of the as deposited molybdenum nitride films, grown at 170 °C, by X-ray photoelectron spectroscopy (XPS). To avoid surface contaminants, all analyses were performed after 3−5 nm etching with Ar plasma under UHV condition. The doublet of Mo3d peaks at 232.3 eV ($3d_{5/2}$) and at 235.5 eV ($3d_{3/2}$), as shown in Figure 6a, confirmed the presence of Mo^{+6}.[56,57] Also the N1s peak position at 397.9 eV, as shown in Figure 6b, strongly justified the chemical nature of the as deposited film as molybdenum nitride.[58]

The atomic ratio between Mo and N was calculated by finding out the percentage of normalized area under the characteristic peaks of individual element divided by the sensitivity factor of the respective peak. The calculated ratio between Mo and N (Mo/N) came out to be ca. 2.1:1. The XPS results indicated that the chemical composition of the as deposited molybdenum nitride films could be Mo_2N.

Electrochemical Characterization. The interest of transition metal nitrides arises from the fact that, in MoN_x, Li ion can intercalate first and later on undergo conversion reaction. During the processes, a large number of lithium ion can be stored at low potential which is an attractive signature for lithium battery anode. A well-anticipated reaction for molybdenum nitrides that react with Li can be written as follows

$$MoN_x + zLi \rightarrow Li_zMoN_x$$

(intercalation reaction; at ∼1.2 V)

$$MoN_x + yLi \rightarrow Mo + xLi_yN$$

(conversion reaction; at ∼0.4 V)

The cyclic voltammogram, as shown in Figure 7, demonstrated a stable electrochemical performance of ALD grown molybdenum nitride thin film. During the first cathodic process, three distinct peaks are observed at 1.0, 0.39, and 0.15 V vs. Li/Li^+. The origin of the peak at 1.0 V could be due to the Li ion intercalation into the bulk of the material.

After the 5th cycle, a new peak appeared at 1.39 V. The origin of this peak is not yet understood. Similar to other metal nitrides,[40,44] the peak at 0.39 V could be attributed to the conversion reaction of molybdenum nitride with Li. This

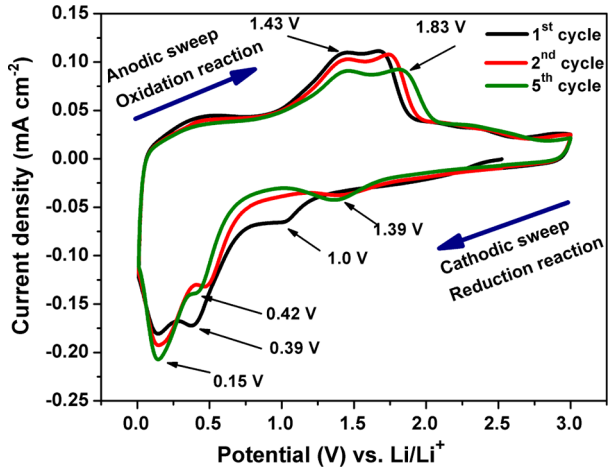

Figure 7. Cyclic voltammogram of MoN_x at a scan rate of 0.2 mV S^{-1} within a potential window of 3.0 to 0.01 V vs. Li/Li^+.

conversion peak shifted to a higher potential (0.42 V) upon cycling probably due to the not-so-easy Li intercalation into residual molybdenum nitride that was embedded in a different chemical environment. Furthermore, the peak at 0.15 V vs. Li/Li^+ is due to solid electrolyte interface (SEI) formation.[59,60] During the anodic sweep, a broad shoulder was observed at ∼0.4 V vs. Li/Li^+ which is due to the breakage of SEI layer. We presume here that the de-lithiation process occurred via two-step reactions that are observed at 1.43 and 1.83 V vs. Li/Li^+, respectively. Another broad shoulder is observed at ∼2.3 V vs. Li/Li^+ which is assigned to the de-intercalation process. A similar kind of voltammogram was also found for other nitride materials such as CoN and VN.[40,44]

Reaction chemistry of metal nitrides with Li was not well studied. To understand the chemistry behind the charge−discharge process that occurred in the cell, continuous electrochemical impedance spectroscopy (EIS) was carried out in the present study. During the entire experiment, cell was not disconnected from the circuit. EIS measurements were performed at four different potentials during both charging and discharging processes as shown in Figure 8. During the discharge process, EIS was taken at 2.7 V (OCV), 0.9 V (after intercalation step), 0.3 V (after conversion process), and end of the discharge process, respectively. Similarly, EIS was taken at 1.0 V (before start of the delithiation process), 1.6 V (after first oxidation peak), 2.0 V (after the 2nd oxidation peak), and end of the charge process, respectively. The entire process was

dx.doi.org/10.1021/am500285d | ACS Appl. Mater. Interfaces 2014, 6, 6606−6615

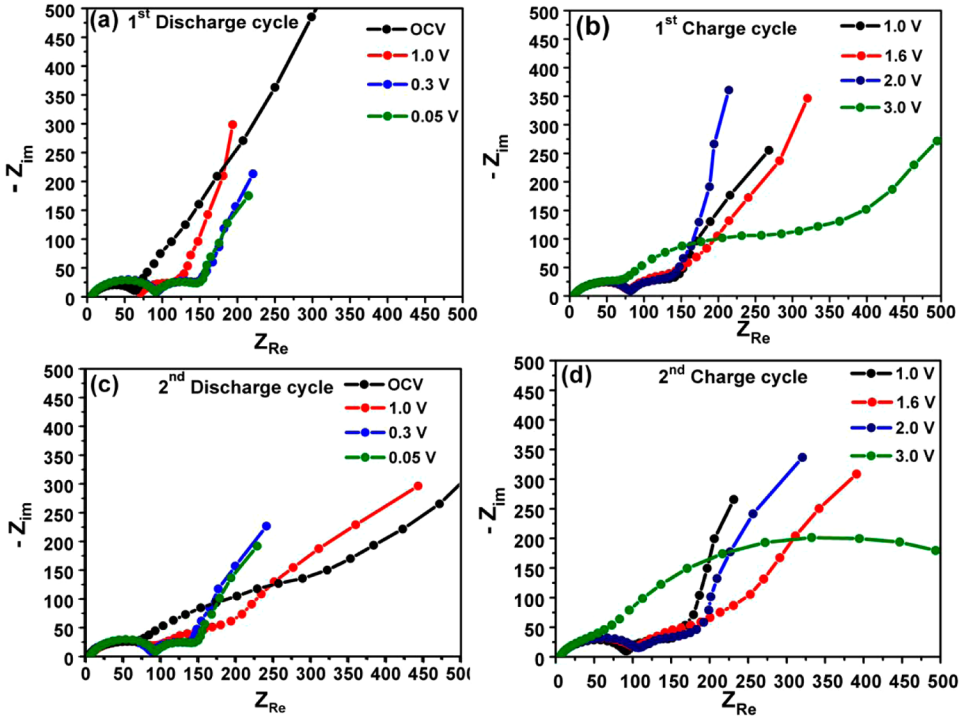

Figure 8. Continuous electrochemical impedance spectroscopy of MoN_x electrode at different potentials during (a) discharge and (b) charge processes for the first cycle; (c) discharge and (d) charge process for the second cycle.

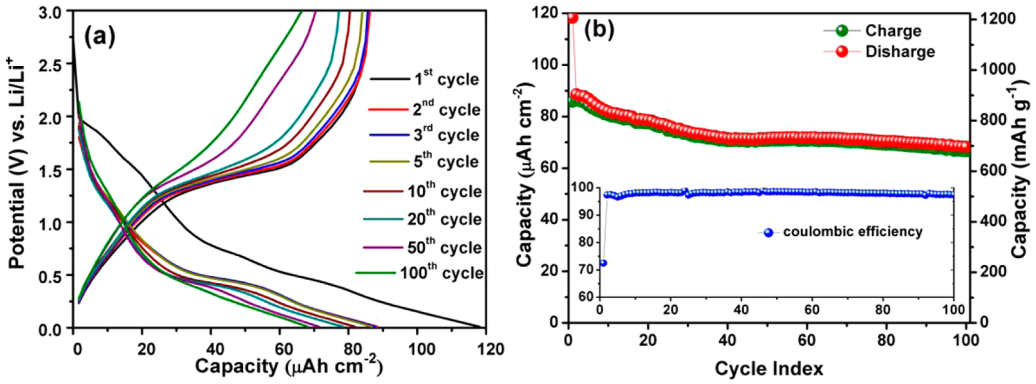

Figure 9. (a) Charge–discharge profile and (b) cyclic performance and coulombic efficiency (inset) of MoN_x from 3.0 to 0.01 V vs. Li/Li^+ at current density of 100 $\mu A\ cm^{-2}$.

repeated for the second cycle to get a better idea of the process and reproducibility. The cell was kept for 24 h after the first cycle to attain the quasi-equilibrium condition.

The Nyquist plot at open circuit voltage showed a depressed semicircle in the high frequency range followed by a slightly inclined line in the low frequency range as shown in Figure 8a. As the electrode potential decreased to 0.9 V, the depressed small semicircle in the high frequency region did not change significantly; however, low frequency dispersion appeared that probably describes the presence of MoN_x–Li_zMoN_x mixed phase.

At the end of the conversion reaction (0.3 V), the semicircle at the low frequency region was nearly unchanged although the intercept of the high frequency semicircle was increased. The increase in the dispersion of the high frequency semicircle is presumed to be due to the formation of SEI layer. The nature of the impedance spectrum remains unchanged while sweeping the potential from 0.3 to 0.01 V, indicating that no more reactions take place in this region. Similarly, during the charging process, the spectrum at 1.0 V showed that there was no change in the low frequency dispersion. However, the dispersion at higher frequency regions was decreased due to the removal of SEI layer. Upon further charging, the nature of both semicircles changed probably due to the formation of molybdenum nitride from Mo nanoparticles and lithium nitrides. At the end of the charging process, the impedance spectrum showed an increase in the low frequency dispersion, which is probably due to the formation of delithiated multiphasic nitride species. Impedance spectra of the second cycle also exhibited a similar observation that showed the robustness of the material.

To investigate the lithium ion battery performance, charge–discharge experiments were performed in half cell configuration. The galvanostatic charge–discharge profiles, shown in Figure 9a, are in good agreement with the cyclic voltammetry results.

dx.doi.org/10.1021/am500285d | ACS Appl. Mater. Interfaces 2014, 6, 6606–6615

Two prominent plateaus (around 1.3 and 0.5 V vs. Li/Li^+) were observed during the discharge process while only one prominent plateau at around 1.4 V was observed in the charging process. Since the charge−discharge experiments are performed at high current rate, very minute redox signature might not appear. The material exhibited excellent cyclic stability during the galvanostatic charge−discharge process, shown in Figure 9b. The cell was tested at a constant current density of 100 $\mu A\ cm^{-2}$. A discharge capacity of 118 $\mu Ah\ cm^{-2}$ is achieved during the first discharge. At the end of 100 cycles, a discharge capacity of 68 $\mu Ah\ cm^{-2}$ equivalent to 696 $mAh\ g^{-1}$ was achieved. High coulombic efficiency of ∼98% was maintained throughout the cycling.

The present work highlights two important factors, (a) a new synthesis scheme to grow molybdenum nitride and (b) demonstration of the MoN_x as a free-standing anode for lithium ion battery application. Molybdenum nitride is deposited for the first time using $Mo(CO)_6$ as a molybdenum source. The two major advantages achieved by introducing this metal hexacarbonyl precursor are the lowest ALD temperature window for the growth and a reasonably high growth rate. While the temperature window for this precursor lies between 150 and 165 °C, it was reported as high as 500 °C for $MoCl_5$ and 250−300 °C in the case of bis(tert-butylimido)-bis(diethyl-(isopropyl)amido)-molybdenum $[(tBuN)_2Mo(NEt_2)_2]$ as a molybdenum source.[26,27] The low temperature window makes the room wider for this material to be used in different applications. The self-limiting growth rate of 2 Å per cycle is also the maximum as per the best of our knowledge for ALD grown molybdenum nitride film. The application of ALD grown molybdenum nitride as anode material itself enriched the literature in two different ways. First, a new material is introduced, and secondly, a different electrode fabrication process was employed. Molybdenum nitride, which was reported for the first time as conversion based anode material for lithium ion battery, exhibits stable electrochemical performance for 50 cycles. A similar kind of electrochemistry was achieved for only a few metal nitrides such as CoN, TiN, VN, and CrN while the rest of the metal nitrides exhibits moderate to poor electrochemistry.[34,35,39−49] In terms of the electrode fabrication process, ALD based electrode preparations are entirely different than the conventional electrode preparation method described elsewhere.[61] In most of the literature, the ALD technique was used to form a protective coating on the active material or to produce nanostructured materials using different templates such as AAO, CNT, graphene, etc.[62] In this present work, active material was directly grown on the stainless steel substrate which is different than the other fabrication techniques. Due to large differences in material composition as well as electrode fabrication, it will not be well justified to compare the present work with the reported results.

CONCLUSIONS

In this paper, we demonstrated atomic layer deposition of molybdenum nitride films using molybdenum hexacarbonyl and ammonia. Film growth and deposition chemistry was studied by *in situ* QCM and FTIR spectroscopy. For the first time, as grown amorphous films were successfully tested as an anode material in Li ion batteries in comparison to the existing literature where molybdenum nitride was used only to enhance the electronic conductivity but never as the active material. As a binder and carbon free electrode, the ALD grown molybdenum nitride films offered high stability during the electrochemical charge−discharge cycle. The reaction chemistry was studied using electrochemical impedance spectroscopy. A reversible conversion reaction during electrochemical cycling was highly evident.

ASSOCIATED CONTENT

Supporting Information

Figure showing the complete survey of the XPS for the as deposited film. This material is available free of charge via the Internet at http://pubs.acs.org.

AUTHOR INFORMATION

Corresponding Authors

*E-mail: shaibal.sarkar@iitb.ac.in.
*E-mail: sagar.mitra@iitb.ac.in.

Author Contributions

†D.K.N. and U.K.S. contributed equally.

Notes

The authors declare no competing financial interest.

ACKNOWLEDGMENTS

This work was supported by the National Centre for Photovoltaic Research and Education (NCPRE) funded by the Ministry of New and Renewable Energy, Govt. of India.

REFERENCES

(1) Zhang, Y. Y.; Haberkorn, N.; Ronning, F.; Wang, H. Y.; Mara, N. A.; Zhuo, M. J.; Chen, L.; Lee, J. H.; Blackmore, K. J.; Bauer, E.; Burrell, A. K.; McCleskey, T. M.; Hawley, M. E.; Schulze, R. K.; Tajima, L. T.; Jia, Q. X. Epitaxial Superconducting delta-MoN Films Grown by a Chemical Solution Method. *J. Am. Chem. Soc.* **2011**, *133*, 20735−20737.

(2) Inumaru, K.; Baba, K.; Yamanaka, S. Synthesis and Characterization of Superconducting beta-Mo_2N Crystalline Phase on a Si Substrate: An Application of Pulsed Laser Deposition to Nitride Chemistry. *Chem. Mater.* **2005**, *17*, 5935−5940.

(3) Wang, L. B.; Tang, K. B.; Zhu, Y. C.; Li, Q. W.; Zhu, B. C.; Wang, L. C.; Si, L. L.; Qian, Y. T. Solid State Synthesis of a New Ternary Nitride $MgMoN_2$ Nanosheets and Micromeshes. *J. Mater. Chem.* **2012**, *22*, 14559−14564.

(4) Chuang, J. C.; Tu, S. L.; Chen, M. C. Sputter-deposited Mo and Reactively Sputter-deposited Mo-N Films as Barrier Layers Against Cu Diffusion. *Thin Solid Films* **1999**, *346*, 299−306.

(5) Alen, P.; Ritala, M.; Arstila, K.; Keinonen, J.; Leskela, M. Atomic Layer Deposition of Molybdenum Nitride Thin Films for Cu Metallizations. *J. Electrochem. Soc.* **2005**, *152*, G361−G366.

(6) Wang, L. X.; Sun, J. C.; Li, P. B.; Sun, J.; Lv, Y.; Jing, B.; Li, S.; Ji, S. J.; Wen, Z. S. Molybdenum Nitride Modified AISI 304 Stainless Steel Bipolar Plate for Proton Exchange Membrane Fuel Cell. *Int. J. Hydrogen Energy* **2012**, *37*, 5876−5883.

(7) Zhang, G. J.; Fan, T. X.; Wang, T.; Chen, H. L. Microstructure, Mechanical and Tribological Behavior of MoN_x/SiN_x Multilayer Coatings Prepared by Magnetron Sputtering. *Appl. Surf. Sci.* **2013**, *274*, 231−236.

(8) Zhu, X. D.; Yue, D.; Shang, C.; Fan, M. T.; Hou, B. Phase Composition and Tribological Performance of Molybdenum Nitride Coatings Synthesized by IBAD. *Surf. Coat. Technol.* **2013**, *228*, S184−S189.

(9) Aghababazadeh, R.; Mirhabibi, A. R.; Pilehvari, S.; Brydson, R. Bench Scale Production of Pure Nanocrystalline Molybdenum Nitride Through Solid-Gas Phase Reduction. *J. Nanosci. Nanotechnol.* **2012**, *12*, 9230−9233.

(10) Wang, H. M.; Wu, Z. J.; Kong, J.; Wang, Z. Q.; Zhang, M. H. Synthesis of Transition Metal Nitride by Nitridation of Metastable Oxide Precursor. *J. Solid State Chem.* **2012**, *194*, 238−244.

(11) Cardenas-Lizana, F.; Lamey, D.; Gomez-Quero, S.; Perret, N.; Kiwi-Minsker, L.; Keane, M. A. Selective Three-phase Hydrogenation of Aromatic Nitro-compounds Over Beta-molybdenum Nitride. *Catal. Today* **2011**, *173*, 53−61.
(12) Nagai, M.; Nakauchi, R. CVD Preparation of Silica-supported Molybdenum Nitride and Its Activity for Thiophene Hydrodesulfurization. *Silic. Ind.* **2004**, *69*, 61−67.
(13) Kadono, T.; Kubota, T.; Okamoto, Y. Hydrodesulfurization over Intrazeolite Molybdenum Nitride Clusters Prepared by Using Hexacarbonyl Molybdenum as a Precursor. *Catal. Today* **2003**, *87*, 107−115.
(14) George, S. M. Atomic Layer Deposition: An Overview. *Chem. Rev.* **2010**, *110*, 111−131.
(15) McCormick, J. A.; Rice, K. P.; Paul, D. F.; Weimer, A. W.; George, S. M. Analysis of Al_2O_3 Atomic Layer Deposition on ZrO_2 Nanoparticles in a Rotary Reactor. *Chem. Vap. Deposition* **2007**, *13*, 491−498.
(16) Alnes, M. E.; Monakhov, E.; Fjellvag, H.; Nilsen, O. Atomic Layer Deposition of Copper Oxide using Copper(II) Acetylacetonate and Ozone. *Chem. Vap. Deposition* **2012**, *18*, 173−178.
(17) Lindahl, E.; Ottosson, M.; Carlsson, J. O. Atomic Layer Deposition of NiO by the Ni(thd)2/H_2O Precursor Combination. *Chem. Vap. Deposition* **2009**, *15*, 186−191.
(18) Short, A.; Jewell, L.; Doshay, S.; Church, C.; Keiber, T.; Bridges, F.; Carter, S.; Alers, G. Atomic Layer Deposition of Zinc Sulfide with Zn(TMHD)2. *J. Vac. Sci. Technol., A* **2013**, *31*, 01A138.
(19) Bakke, J. R.; Jung, H. J.; Tanskanen, J. T.; Sinclair, R.; Bent, S. F. Atomic Layer Deposition of CdS Films. *Chem. Mater.* **2010**, *22*, 4669−4678.
(20) Wedemeyer, H.; Michels, J.; Chmielowski, R.; Bourdais, S.; Muto, T.; Sugiura, M.; Dennler, G.; Bachmann, J. Nanocrystalline Solar Cells with an Antimony Sulfide Solid Absorber by Atomic Layer Deposition. *Energy Environ. Sci.* **2013**, *6*, 67−71.
(21) Lee, H. B. R.; Park, Y. J.; Baik, S.; Kim, H. Initial Stage Growth during Plasma-Enhanced Atomic Layer Deposition of Cobalt. *Chem. Vap. Deposition* **2012**, *18*, 41−45.
(22) Seghete, D.; Rayner, G. B.; Cavanagh, A. S.; Anderson, V. R.; George, S. M. Molybdenum Atomic Layer Deposition Using MoF_6 and Si_2H_6 as the Reactants. *Chem. Mater.* **2011**, *23*, 1668−1678.
(23) George, S. M.; Lee, B. H.; Yoon, B.; Abdulagatov, A. I.; Hall, R. A. Metalcones: Hybrid Organic-Inorganic Films Fabricated Using Atomic and Molecular Layer Deposition Techniques. *J. Nanosci. Nanotechnol.* **2011**, *11*, 7948−7955.
(24) Lee, B. H.; Yoon, B.; Abdulagatov, A. I.; Hall, R. A.; George, S. M. Growth and Properties of Hybrid Organic-Inorganic Metalcone Films Using Molecular Layer Deposition Techniques. *Adv. Funct. Mater.* **2013**, *23*, 532−546.
(25) Yoon, B.; Seghete, D.; Cavanagh, A. S.; George, S. M. Molecular Layer Deposition of Hybrid Organic-Inorganic Alucone Polymer Films Using a Three-Step ABC Reaction Sequence. *Chem. Mater.* **2009**, *21*, 5365−5374.
(26) Hiltunen, L.; Leskela, M.; Makela, M.; Niinisto, L.; Nykanen, E.; Soininen, P. Nitrides of Titanium, Niobium, Tantalum and Molybdenum Grown as Thin-films by the Atomic Layer Epitaxy Method. *Thin Solid Films* **1988**, *166*, 149−154.
(27) Miikkulainen, V.; Suvanto, M.; Pakkanen, T. A. Bis(tert-butylimido)-bis(dialkylamido) Complexes of Molybdenum as Atomic Layer Deposition (ALD) Precursors for Molybdenum Nitride: The Effect of the Alkyl Group. *Chem. Vap. Deposition* **2008**, *14*, 71−77.
(28) Diskus, M.; Nilsen, O.; Fjellvag, H. Growth of Thin Films of Molybdenum Oxide by Atomic Layer Deposition. *J. Mater. Chem.* **2011**, *21*, 705−710.
(29) Diskus, M.; Balasundaram, M.; Nilsen, O.; Fjellvag, H. Influence of Precursors Chemistry on ALD Growth of Cobalt-molybdenum Oxide Films. *Dalton Trans.* **2012**, *41*, 2439−2444.
(30) Elder, S. H.; Doerrer, L. H.; DiSalvo, F. J.; Parise, J. B.; Guyomard, D.; Tarascon, J. M. $LiMoN_2$: The First Metallic Layered Nitride. *Chem. Mater.* **1992**, *4*, 928−937.
(31) Nishijima, M.; Kagohashi, T.; Imanishi, M.; Takeda, Y.; Yamamoto, O.; Kondo, S. Synthesis and Electrochemical Studies of a New Anode Material, $Li_{3-x}Co_xN$. *Solid State Ionics* **1996**, *83*, 107−111.
(32) Shodai, T.; Okada, S.; Tobishima, S.; Yamaki, J. Study of Li1-xMxN (M: Co, Ni or Cu) System for Use as Anode Material in Lithium Rechargeable Cells. *Solid State Ionics* **1996**, *86-88*, 785−789.
(33) Poizot, P.; Laruelle, S.; Grugeon, S.; Dupont, L.; Tarascon, J. M. Nano-sized Transition-metal Oxides as Negative-electrode Materials for Lithium-ion Batteries. *Nature* **2000**, *407*, 496−499.
(34) Pereira, N.; Klein, L. C.; Amatucci, G. G. The Electrochemistry of Zn_3N_2 and LiZnN - A Lithium Reaction Mechanism for Metal Nitride Electrodes. *J. Electrochem. Soc.* **2002**, *149*, A262−A271.
(35) Pereira, N.; Balasubramanian, M.; Dupont, L.; McBreen, J.; Klein, L. C.; Amatucci, G. G. The Electrochemistry of Germanium Nitride with Lithium. *J. Electrochem. Soc.* **2003**, *150*, A1118−A1128.
(36) Gillot, F.; Boyanov, S.; Dupont, L.; Doublet, M. L.; Morcrette, A.; Monconduit, L.; Tarascon, J. M. Electrochemical Reactivity and Design of NiP_2 Negative Electrodes for Secondary Li-Ion Batteries. *Chem. Mater.* **2005**, *17*, 6327−6337.
(37) Sen, U.K.; Sarkar, S.; Veluri, P.S.; Singh, S.; Mitra, S. Nano Dimensionality: A Way towards Better Li-Ion Storage. *Nanosci. Nanotechnol. Asia* **2013**, *3*, 21−35.
(38) Gregory, D. H.; O'Meara, P. M.; Gordon, A. G.; Hodges, J. P.; Short, S.; Jorgensen, J. D. Structure of Lithium Nitride and Transition-metal-doped Derivatives, $Li_{3-x-y}M_xN$ (M = Ni, Cu): A Powder Neutron Diffraction Study. *Chem. Mater.* **2002**, *14*, 2063−2070.
(39) Fu, Z. W.; Wang, Y.; Yue, X. L.; Zhao, S. L.; Qin, Q. Z. Electrochemical Reactions of Lithium with Transition Metal Nitride Electrodes. *J. Phys. Chem. B* **2004**, *108*, 2236−2244.
(40) Sun, Q.; Fu, Z. W. Vanadium Nitride as a Novel Thin Film Anode Material for Rechargeable Lithium Batteries. *Electrochim. Acta* **2008**, *54*, 403−409.
(41) Zhang, K.; Wang, H.; He, X.; Liu, Z.; Wang, L.; Gu, L.; Xu, H.; Han, P.; Dong, S.; Zhang, C.; Yao, J.; Cui, G.; Chen, L. A Hybrid Material of Vanadium Nitride and Nitrogen-doped Graphene for Lithium Storage. *J. Mater. Chem.* **2011**, *21*, 11916−11922.
(42) Gillot, F.; Solé, J. O.; Palacín, M. R. Nickel Nitride as Negative Electrode Material for Lithium Ion Batteries. *J. Mater. Chem.* **2011**, *21*, 9997−10002.
(43) Yue, Y.; Han, P.; He, X.; Zhang, K.; Liu, Z.; Zhang, C.; Dong, S.; Gu, L.; Cui, G. In Situ Synthesis of a Graphene/Titanium Nitride Hybrid Material with Highly Improved Performance for Lithium Storage. *J. Mater. Chem.* **2012**, *22*, 4938−4943.
(44) Das, B.; Reddy, M. V.; Subba Rao, G. V.; Chowdari, B. V. R. Synthesis of Porous-CoN Nanoparticles and Their Application as a High Capacity Anode for Lithium-ion Batteries. *J. Mater. Chem.* **2012**, *22*, 17505−17510.
(45) Das, B.; Reddy, M. V.; Rao, G. V. S.; Chowdari, B. V. R. Synthesis and Li-storage Behavior of CrN Nanoparticles. *RSC Adv.* **2012**, *2*, 9022−9028.
(46) Veith, G. M.; Baggetto, L.; Adamczyk, L. A.; Guo, B.; Brown, S. S.; Sun, X. G.; Albert, A. A.; Humble, J. R.; Barnes, C. E.; Bojdys, M. J.; Dai, S.; Dudney, N. J. Electrochemical and Solid-State Lithiation of Graphitic C_3 N_4. *Chem. Mater.* **2013**, *25*, 503−508.
(47) Reddy, M. V.; Prithvi, G.; Loh, K. P.; Chowdari, B. V. R. Li Storage and Impedance Spectroscopy Studies on Co_3O_4, CoO, and CoN for Li-Ion Batteries. *ACS Appl. Mater. Interfaces* **2014**, *6*, 680−690.
(48) Baggetto, L.; Verhaegh, N. A. M.; Niessen, R. A. H.; Roozeboom, F.; Jumas, J. C.; Notten, P. H. L. Tin Nitride Thin Films as Negative Electrode Material for Lithium-Ion Solid-State Batteries. *J. Electrochem. Soc.* **2010**, *157*, A340−A347.
(49) Bouhtiyya, S.; Porto, R. L.; Laïk, B.; Boulet, P.; Capon, F.; Ramos, J.P. P.; Brousse, T.; Pierson, J.F. Application of Sputtered Ruthenium Nitride Thin Films as Electrode Material for Energy-storage Devices. *Scr. Mater.* **2013**, *68*, 659−662.
(50) Liu, J.; Tang, S.; Lu, Y.; Cai, G.; Liang, S.; Wang, W.; Che, X. Synthesis of Mo_2N Nanolayer Coated MoO_2 Hollow Nanostructures

as High-performance Anode Materials for Lithium-ion Batteries. *Energy Environ. Sci.* **2013**, *6*, 2691−2697.
(51) Yoon, S.; Jung, K. N.; Jin, C. S.; Shin, K. H. Synthesis of Nitrided MoO_2 and Its Application as Anode Materials for Lithium-ion Batteries. *J. Alloys Compd.* **2012**, *536*, 179−183.
(52) Zhou, D.; Wu, H.; Wei, Z.; Han, B. H. Graphene−molybdenum Oxynitride Porous Material with Improved Cyclic Stability and Rate Capability for Rechargeable Lithium-ion Batteries. *Phys. Chem. Chem. Phys.* **2013**, *15*, 16898−16906.
(53) Ji, W.; Shen, R.; Yang, R.; Yu, G.; Guo, X.; Peng, L.; Ding, W. Partially Nitrided Molybdenum Trioxide with Promoted Performance as an Anode Material for Lithium-ion Batteries. *J. Mater. Chem. A* **2014**, *2*, 699−704.
(54) Kurhinen, M.; Venalainen, T.; Pakkanen, T. A. Subcarbonyl Species of Molybdenum Hexacarbonyl Supported on Silica - A Drift Study. *J. Phys. Chem.* **1994**, *98*, 10237−10242.
(55) Burton, B. B.; Lavoie, A. R.; George, S. M. Tantalum Nitride Atomic Layer Deposition Using (tert-butylimido) tris(diethylamido) Tantalum and Hydrazine. *J. Electrochem. Soc.* **2008**, *155*, D508−D516.
(56) Ghampsona, I. T.; Sepúlveda, C.; Garciac, R.; Radovic, L. R.; Fierro, J. L. G.; DeSistoa, W. J.; Escalona, N. Hydrodeoxygenation of Guaiacol over Carbon-supported Molybdenum Nitride Catalysts: Effects of Nitriding Methods and Support Properties. *Appl. Catal., A: Gen.* **2012**, *439*, 111−124.
(57) Yang, S.; Li, C.; Xu, J.; Xin, Q. Surface Sites of Alumina-supported Molybdenum Nitride Characterized by FTIR, TPD-MS, and Volumetric Chemisorption. *J. Phys. Chem. B* **1998**, *102*, 6986−6993.
(58) Nagai, M.; Irisawa, A.; Omi, S. XPS Study of the Deactivation and Sulfiding of Nitrided Molybdena-alumina Catalyst During the Hydrodesulfurization of Dibenzothiophene. *J. Phys. Chem. B* **1998**, *102*, 7619−7626.
(59) Wang, F. M.; Yu, M. H.; Hsiao, Y. J.; Tsai, Y.; Hwang, B. J.; Wang, Y. Y.; Wan, C. C. Aging Effects to Solid Electrolyte Interface (SEI) Membrane Formation and the Performance Analysis of Lithium Ion Batteries. *Int. J. Electrochem. Sci.* **2011**, *6*, 1014−1026.
(60) Abe, K.; Yoshitake, H.; Kitakura, T.; Hattori, T.; Wang, H.; Yoshio, M. Additives-containing Functional Electrolytes for Suppressing Electrolyte Decomposition in Lithium-ion Batteries. *Electrochim. Acta* **2004**, *49*, 4613−4622.
(61) Marks, T.; Trussler, S.; Smith, A. J.; Xiong, D.; Dhan, J. R. A Guide to Li-Ion Coin-Cell Electrode Making for Academic Researchers. *J. Electrochem. Soc.* **2011**, *158*, A51−A57.
(62) Meng, X.; Yang, X. Q.; Sun, X. Emerging Applications of Atomic Layer Deposition for Lithium-Ion Battery Studies. *Adv. Mater.* **2012**, *24*, 3589−3615.